Journal of Materials Chemistry

Cite this: *J. Mater. Chem.*, 2011, **21**, 5238

www.rsc.org/materials

PAPER

Fluorenone core donor–acceptor–donor π-conjugated molecules end-capped with dendritic oligo(thiophene)s: synthesis, liquid crystalline behaviour, and photovoltaic applications†

Frédéric Lincker,[a] Benoît Heinrich,[c] Rémi De Bettignies,[b] Patrice Rannou,[a] Jacques Pécaut,[d] Benjamin Grévin,[a] Adam Pron,[a] Bertrand Donnio*[c] and Renaud Demadrille*[a]

Received 27th July 2010, Accepted 16th December 2010
DOI: 10.1039/c0jm02437f

We have synthesized a new series of donor–acceptor–donor (D–A–D) π-conjugated molecules, consisting of fluorenone core end-capped with dendritic oligo(thiophene)s of increasing generation (abbreviated as **FG0**, **FG1**, and **FG2**). In view of the application of these new organic semiconductors in photovoltaic devices, we have explored their spectroscopic, redox, and structural properties. The thermal behaviour of the new organic semiconductors was investigated by differential scanning calorimetry and polarized-light optical microscopy. Liquid crystalline behaviour has been found in the case of **FG1**, corresponding to a smectic ordering with a triclinic symmetry (Sm_{obl}) upon heating, as confirmed by variable temperature small-angle X-ray diffraction studies. In order to evaluate their photovoltaic performances, devices with an active area of 0.28 cm^2 were fabricated. Under AM1.5 simulated sunlight (100 mW cm^{-2}) conditions, a device containing **FG1**/[70]PCBM blends showed a power conversion efficiency of *ca.* 0.8%.

1. Introduction

Organic semiconducting materials showing efficient opto-electronic and modulable self-organisation properties have been the focus of an impressive number of studies during the past two decades because of their integration as electroactive components into photovoltaic cells,[1] light-emitting diodes[2] or field-effect transistors.[3] Among these applications, organic semiconductors are of particular interest for the fabrication of bulk-heterojunction (BHJ) solar cells.[4] Among others, this interest relies on their ease to process which facilitates the fabrication of large area, flexible, quasi defect-free (*e.g.* self-healing), and low-cost modules.[5] Up to now, BHJ organic solar cells based on solution-processed materials have been dominated by polymers. However recently, the concept of molecular BHJ has been introduced,[6] and several research groups have reported promising photovoltaic performances for organic solar cells in which the active layer was prepared by solution processing.[7] Molecular electron-donating materials reveal several advantages, as compared to their polymeric counterparts, in terms of synthesis, purification, simplicity of processing, and tuning of their chemical structure.[8] Lately, dendritic materials or hyperbranched π-conjugated compounds have been successfully employed as electron donor components in BHJ organic solar cells.[9] It has been clearly demonstrated that increasing the size of oligo(thiophene) dendrons (*i.e.* their generation number), used for the preparation of the thiophene-based dendrimers, resulted in a systematic increase in device performance, which was hypothesised to originate from an improvement of the carrier's mobility.[10] On the other hand, thiophene-based dendrimers usually present large band gap, as compared to linear systems of comparable polymerization degree. This observation can be explained by the limited electronic π-conjugation originating from the steric hindrance and twisting between the adjacent thiophene units. Therefore, strategies to decrease the band gap of these materials and, as a consequence, to improve their light-harvesting properties, have attracted the attention of several research groups.[11]

Our group has recently reported the preparation and application in a bulk-heterojunction organic solar cell of a new class of small molecules containing fluorenone units. Devices containing these compounds blended with [60]PCBM yielded a maximum power conversion efficiency of 1.2%. Motivated by these results

[a]*CEA-INAC-UMR5819-SPrAM (CEA/CNRS/UJF), Laboratoire d'Electronique Moléculaire Organique et Hybride, 17, Rue des Martyrs, F-38054 Grenoble, France. E-mail: renaud.demadrille@cea.fr*
[b]*INES-CEA-RDI-DTS, Laboratoire Cellules Solaires, Le Bourget du Lac, Technolac Chambéry, F-73370, France. E-mail: remi.de-bettignies@cea.fr*
[c]*IPCMS-UMR 7504, CNRS-Université de Strasbourg, 23, rue du Læss BP 43, Strasbourg Cedex 2, F-67034, France. E-mail: bdonnio@ipcms.u-strasbg.fr*
[d]*CEA-INAC-SCIB, Reconnaissance Ionique et Chimie de Coordination, 17, Rue des Martyrs, F-38054 Grenoble, France*

† Electronic supplementary information (ESI) available: Details related to the solar cell device fabrication, analytical and synthetic procedures of chemical intermediates, used chemicals, crystal data of compound **8**, SEC elugrams of **FGX**, **3-G1**, and **5-G2**, and XRD patterns of **FG1**. See DOI: 10.1039/c0jm02437f

and inspired by the investigations on dendritic materials reported by other groups, we have focused our attention on the design and the synthesis of donor–acceptor molecules containing a fluorenone central unit symmetrically coupled to oligo(thiophene) segments end-capped with dendritic oligo(thiophene) wedges. A combination of alkylated oligothiophene dendrons attached to a fluorenone central unit *via* a linear oligo(thiophene) linker is expected to provide highly soluble materials showing an extended absorption spectral range in the visible part thanks to the emergence of an internal charge-transfer (ICT) absorption band.[12] On the other hand, the electron affinity of the fluorenone unit and the electron releasing character of the oligo(thiophene) segments should in principle lead to a molecular system whose frontier orbital HOMO and LUMO are well-positioned with regard to those of [60]PCBM, allowing the occurrence of the photo-induced charge transfer between the two semiconductors. Herein, we present the synthesis of such molecules containing end-capping oligothiophene dendrons up to the second generation. We also report on their optical and electrochemical behaviour. In order to optimise the fabrication of organic optoelectronic devices, it is highly desirable to understand the effect of thermal annealing treatment on the structuration of these compounds. Consequently, their thermal behaviour has also been investigated by differential scanning calorimetry (DSC), polarized-light optical microscopy (POM), and small-angle X-ray diffraction (SAXD). The presence of a mesophase with a triclinic symmetry (Sm_{obl}) was confirmed for the compound based on the first generation of oligo(thiophene) dendron (**FG1**). Finally, we report preliminary results obtained in test photovoltaic cells and demonstrate the applicability of these molecules as donor components in molecular bulk-heterojunction solar cells.

2. Results and discussion

2.1. Material synthesis

The overall synthetic strategy developed thereafter relies on the efficient palladium-catalyzed Stille coupling reaction. The preparation of the symmetric donor–acceptor–donor (D–A–D) type compounds, containing a fluorenone central unit and peripheral thiophene based electron-rich segments, consisted of the direct attachment of the two oligo(thiophene)-based dendron residues at the last stage of the synthetic protocol (orthogonal methodology). Oligo(thiophene) dendrons, up to the second generation (**1-G0**, **3-G1** and **5-G2**, Scheme 1), and their stannyl derivatives (**2**, **4** and **6**, Scheme 1) were synthesized by a convergent synthetic route according to literature methods[13] starting from 2,3-dibromothiophene by iterative palladium-catalyzed cross-coupling reaction. Briefly, 2-stannyl-5-octylthiophene (**2**) was synthesized by treatment of 2-octylthiophene (**1-G0**) with butyllithium and trimethyltin chloride. Due to the high toxicity of trimethyltin derivatives, the crude product was merely washed with ammonium chloride aqueous solution and used without further purification. The dendritic percursor **3-G1** was obtained in excellent yield (88%) by the Stille coupling method between (**2**) and 2,3-dibromothiophene.

Using a similar procedure, **5-G2** compound was obtained in good yields (85%). Compound **3-G1** was readily lithiated using butyllithium and reacted with trimethyltin chloride to give the stannyl compound **4** for the following Stille coupling. An excess of the stannyl compound was used to ensure completion of the coupling reaction with 2,3-dibromothiophene to yield **5-G2**. Derivative **6** was prepared as **2** or **4** from **5-G2**.

For dendrimer synthesis, assembly of dendrons to a core is widely used in order to form functional dendrimers or to simply enlarge the π-conjugated system of the compound. For the preparation of the donor–acceptor–donor (D–A–D) type compounds, we decided to start from a fluorenone-based compound **7**, namely 2,7-bis(4-octyl-5,2'-bithien-2-yl)-fluoren-9-one. This molecule can be prepared in gram-scale according to the procedure described in our previous report.[14] Treating **7** with *N*-bromosuccinimide or *N*-iodosuccinimide gave the corresponding dibromo or diiodo derivatives (**8** and **9**, Scheme 2) in good yields (63% and 74% respectively). Compounds **FG0** (reference compound), **FG1** and **FG2** were then obtained by coupling the dihalogeno derivative **8** or **9** with compounds **2**, **4** and **6**, according to the Stille cross-coupling conditions (Scheme 2). The use of the iodine derivative is highly recommended for the preparation of the dendrimers since it was found that the coupling reaction carried out with the dibromo derivative gives **FG0** in significantly lower yields (50% *vs.* 89%). The fluorenone core-based D–A–D dendrimers were obtained in quite good yields varying from 75% for the smaller one, **FG1**, to 48% for the larger one, **FG2**. It should be noted that the presence of multiple *n*-octyl chains in the final molecules advantageously ensures their high solubility (up to *ca.* 80 g L^{-1}) in common organic solvents,[2] used for the fabrication of organic solar cells, such as chloroform, toluene, cholorobenzene, and *ortho*-dichlorobenzene. The structure and purity of the dendritic precursors **3-G1**, **5-G2** as well as those of the corresponding fluorenone-based **FG0**, **FG1**, and **FG2** D–A–D molecules were confirmed by ^{1}H and ^{13}C NMR spectroscopy, and size-exclusion chromatography (SEC).

2.2. Optical properties

The electronic and optical properties of fluorenone-containing molecules and polymers are usually very different from their fluorene analogues. This is caused by the presence of an additional chromophore (*i.e.* the carbonyl group) giving rise to specific spectral features characteristic of the fluorenone unit. The lowest energy transition in fluorenone possesses n–π* or a π–π* character[15] with a contribution from an internal charge-transfer (ICT) which is responsible for the extension of the absorption bands within the visible part of the spectrum for this class of molecules.[16] In UV-Vis spectra of compounds with a fluorenone-core linked in positions 2 and 7 to oligo(thiophene)s all spectral characteristics, discussed above, can clearly be distinguished.[15,17] They all exhibit two more or less resolved absorption bands. The more intense peak is located at the limit between the UV and the visible parts of the spectrum (*i.e.* $\lambda < 430$ nm in solution) and corresponds to the π–π* transition of the π-conjugated aromatic rings. The longer wavelength band (*i.e.* the band located in the visible part of the spectrum) can be ascribed to an ICT that occurs between the electron rich oligo(thiophene) segments and the central fluorenone unit. The UV-Vis spectra of **FG0**, **FG1** and **FG2** recorded in chloroform

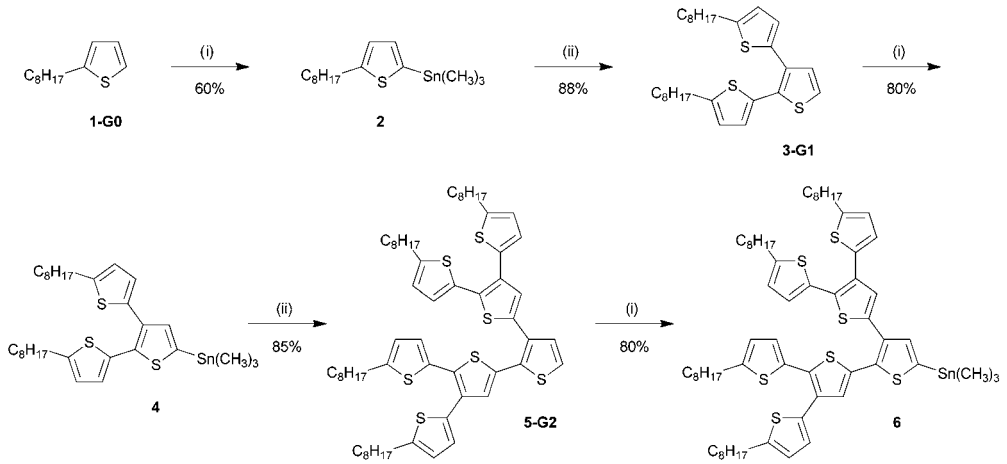

Scheme 1 Synthesis of oligo(thiophene) dendrons **3-G1** and **5-G2**, and stannylated derivatives **2**, **4** and **6**. *Reagents and conditions*: (i) (a) *n*-BuLi, THF, −78 °C to −40 °C, (b) $(CH_3)_3SnCl$, THF, −78 °C to room temperature; (ii) 2,3-dibromothiophene, $Pd(PPh_3)_4$, DMF, 100 °C.

solutions and the solid-state spectra obtained for thin solid films are shown in Fig. 1a and 1b, respectively. With increasing number of thiophene units in the peripheral segments, the position of the maximum absorption peak is bathochromically shifted from 410 nm (**FG0**), to 420 nm (**FG1**) and, to 423 nm (**FG2**) in chloroform solutions; simultaneously the molecular coefficients of absorption for the λ_{max} transition increase. This behaviour is expected since the molar absorption coefficient is known to be dependent upon the number of the thiophene units in linear but also branched oligo(thiophene)s.[18] A broadening of the spectrum is also observed, postulated to originate from the merging of the bathochromically-shifted π–π* absorption band and the ICT one rather than from intermolecular interactions occurring sometimes in highly concentrated solutions.[19] In addition, the higher spectral weight at shorter wavelength in **FG2** is due to the distribution of π-conjugation lengths in the dendritic structure as observed in other thiophene-based dendrimers.[20] In spectra of thin films spin-cast on a glass substrate, an even more pronounced bathochromic shift is observed with increasing number of peripheral thiophene rings. The peaks are broader and

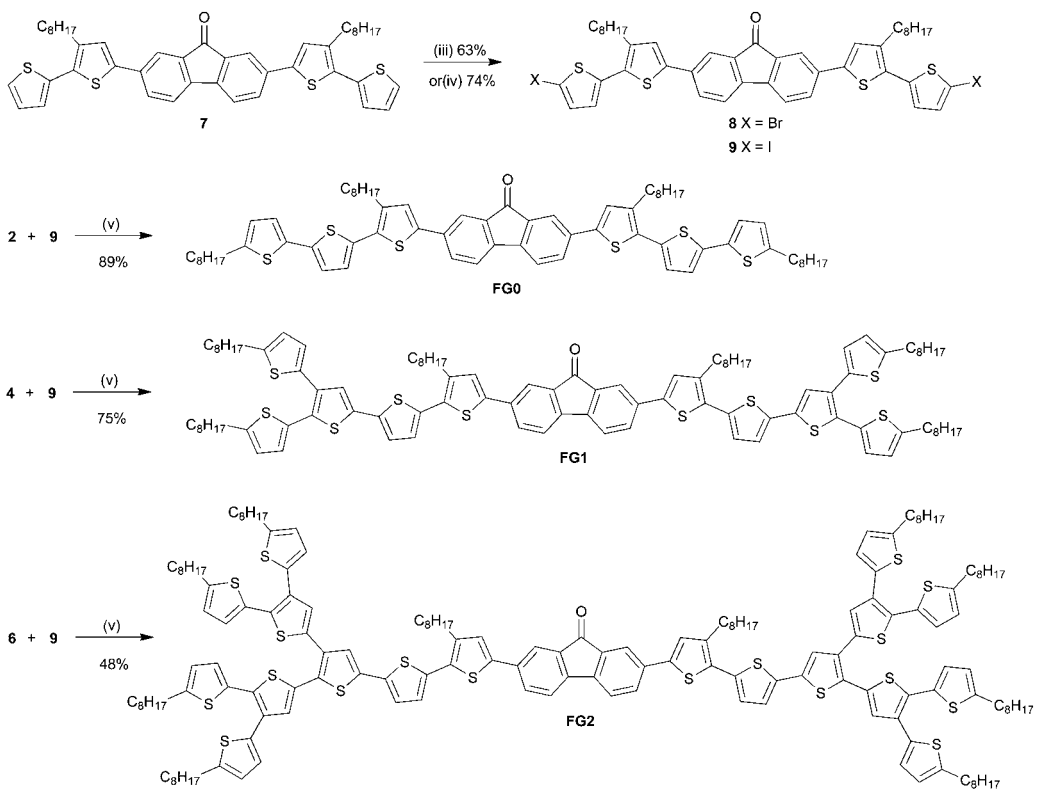

Scheme 2 Synthesis of fluorenone-based intermediates **8** and **9** and fluorenone-thiophene dendrimers **FG0** (reference compound), **FG1** and **FG2**. *Reagents and conditions*: (iii) NBS, $CHCl_3$, room temperature; (iv) NIS, $CHCl_3$, room temperature; (v) $Pd(PPh_3)_4$ DMF, 100 °C.

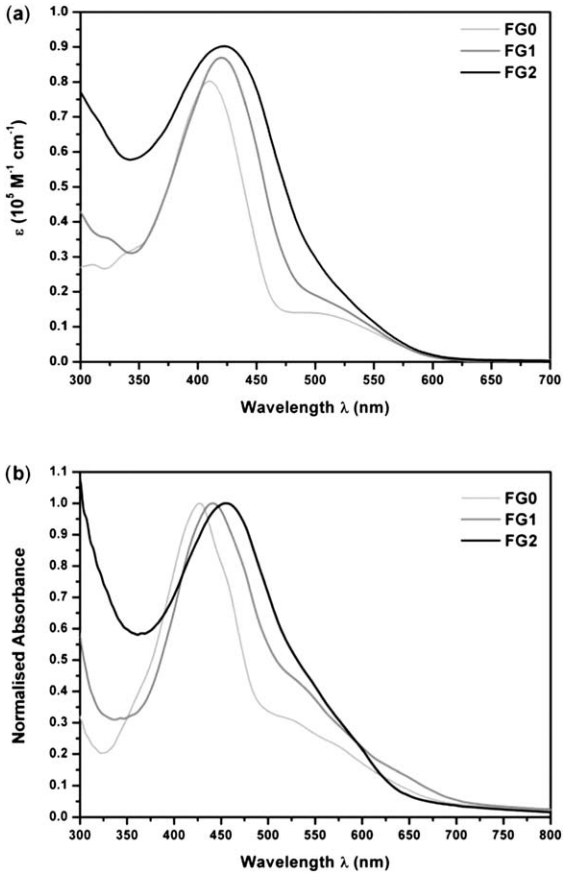

Fig. 1 a) UV-Vis spectra of **FG0**, **FG1**, and **FG2** in chloroform solution. (b) Normalized solid-state UV-Vis spectra of **FG0**, **FG1** and **FG2** thin films cast from chlorobenzene solution.

this broadening can be attributed to intermolecular interactions in the solid state, *i.e.* π–π stacking of the π-conjugated backbones.[21] The steric hindrance of the oligo(thiophene) dendrons in **FG2** leads to reduced intermolecular interactions. This may explain the lower absorption edge (700 nm) for this molecule in the solid-state when compared to that measured for **FG1** (725 nm). The optical band gap was calculated for each compound from the absorption edge of their thin film spectrum. The determined optical band gap values (lying between *ca.* 1.71 and 1.77 eV) were lower that those of the corresponding fluorenone and thiophene-based homo(oligomer)s or homo(polymer)s,[22] indicating a band gap narrowing phenomenon induced by donor–acceptor interactions.

2.3. Electrochemical properties

Cyclic voltammetry or differential pulse voltammetry are important techniques for the investigations of π-conjugated molecules and macromolecules since, in properly executed experiments, the positions of their HOMO and LUMO levels can be estimated and, by consequence, the width of the so-called "electrochemical gap" can be calculated.

Fig. 2 depicts the cyclic voltammograms of **FG0**, **FG1** and **FG2**. The first reduction and first oxidation potentials are listed in Table 1. From these data, the positions of the HOMO and

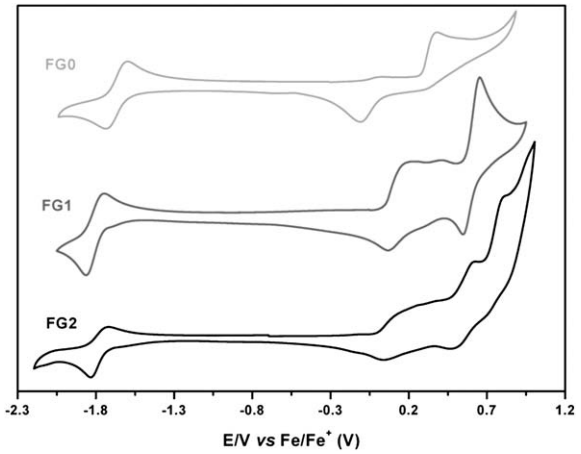

Fig. 2 Cyclic voltammograms showing the first scans of cathodic and anodic polarization of **FG0**, **FG1**, and **FG2** at a scan rate of 20 mV s^{-1}.

LUMO levels were estimated according to a published procedure.[23] The electrochemical band-gap values were calculated as the difference between the positions of the LUMO and HOMO levels. They are in a rather good agreement with the optical band gaps. One should also note that the measured band gaps are lower than those measured for thiophene or fluorenone homo(oligomer)s or homo(polymer)s[23] which, again, can be considered as a manifestation of intramolecular D–A interactions.

Cylic voltammogram of **FG0** shows one anodic peak, corresponding to the oxidation of the oligo(thiophene) moiety, which has its reduction counterpart in the reverse scan. The electron withdrawing character of the fluorenone core causes a significant shift of this oxidation peak towards higher potentials. With increasing size of the end-capping dendrons, the oxidation process becomes multi-step and starts at lower potentials (see voltammograms of **FG1** and **FG2**). It may be postulated that peripheral thiophene rings are better screened from the electron withdrawing effect of the fluorenone core and start to oxidize first.

The two-steps and three-steps oxidation processes of **FG1** and **FG2** are consistent with two types of thiophene rings in the former molecule, and with three different types in the latter one. The reduction process of fluorenone-containing π-conjugated molecules or macromolecules occurs *via* transforming of the carbonyl group to a radical anion.[24]

In **FG0**, **FG1**, and **FG2** this reduction is strongly influenced by electron-donating properties of the oligo(thiophene) substituents and occurs at potentials lowered by *ca.* 200 mV when compared to values observed for fluorenone-based homooligomers and homopolymers.[23] Within the studied series, the electron donating effect is slightly more pronounced in the case of dendrons of generations 1 and 2.

To summarize, increasing the number of thiophene rings has a stronger effect on the oxidation process onset and a weaker effect on the reduction process. As a result the electrochemical band gap decreases with increasing dendron generation.

Taking into account that **FG0**, **FG1**, and **FG2** are potential candidates for the application in BHJ organic solar cells, it is instructive to compare their HOMO and LUMO levels with

Table 1 Optical and electrochemical data of **FG0**, **FG1**, and **FG2**

	Optical data					Electrochemical data				
	Solution[a]		Film[b]							
	λ_{max}/nm	ε (λ_{max}) /M^{-1} cm^{-1}	λ_{max}/nm	λ_{edge}/nm	E_g/eV	E_{ox}[c]/V	E_{red}[c]/V	HOMO/eV	LUMO/eV	E_g/eV
FG0	410	80 200	427	700	1.77	0.33	−1.67	−5.13	−3.13	2.00
FG1	420	86 950	441	725	1.71	0.14	−1.79	−4.94	−3.01	1.93
FG2	423	90 200	455	700	1.77	0.10	−1.77	−4.90	−3.02	1.87

[a] 10^{-5} mol L^{-1} chloroform solution. [b] Spin-coated from a 1.5 wt% chlorobenzene solution. [c] The electrolyte was 0.1 mol L^{-1} $TBAPF_6$/anhydrous CH_2Cl_2 containing 0.5–1.5 × 10^{-3} mol L^{-1} of the corresponding molecule. The standard potentials of the first reduction and the first oxidation peaks (±20 mV) are reported with respect to the Fc/Fc$^+$ couple. The redox potential of Fc/Fc$^+$ which has an absolute energy level of −4.8 eV relative to the vacuum level for calibration is located at 0.15 V in 0.1 M $TBAPF_6$/anhydrous CH_2Cl_2 solution.

those of [70]PCBM and [60]PCBM. The positions of the LUMO levels of [70]PCBM and [60]PCBM were determined from the first reduction peak, using the above described procedure and they were found at −3.8 and −3.9 eV respectively, which is in good agreement with the values reported by other groups.[25]

The LUMO energy levels of the **FGX** (X= 0, 1, and 2) compounds are approximately located at −3.0 eV, which is *ca.* 0.8 to 0.9 eV above the LUMO energy levels of the PCBM-type acceptors. This relative positioning of the frontier orbitals is particularly favorable for the photo-induced electron transfer process.[26]

The HOMO levels, comprised between −5.13 and −4.90 eV, are in a good range to ensure a correct V_{oc} in photovoltaic devices employing [60]PCBM or [70]PCBM as the electron acceptor components.

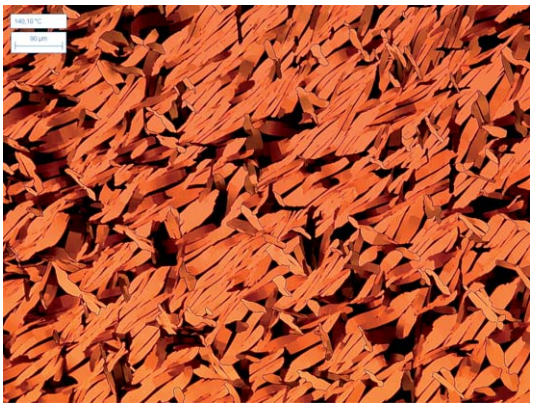

Fig. 3 Representative polarized optical microphotograph of the texture of the mesophase shown by **FG1** at 140 °C and obtained by applying a slow cooling (0.5 °C min^{-1}) from the isotropic phase.

2.4. Liquid crystalline properties

Prior to investigating the applicability of our new materials for uses in BHJ organic solar cells, we investigated their condensed state phase structures and thermal transitions. The thermal behaviour of **FG0**, **FG1**, and **FG2** compounds was investigated using DSC, POM, and SAXD. DSC traces of compounds **FG0** and **FG2** revealed sharp transitions peaks at 155 and 34 °C, respectively, provisionally attributed to crystal-to-isotropic liquid transition. On cooling, these transitions are considerably shifted (supercooling effect). The absence of mesophase for **FG0** and **FG2** was confirmed by POM observations and SAXD. In contrast, DSC traces of **FG1** were characterized by two peaks (observed at 126 and 159 °C during heating scans), fully reversible on both heating and cooling (Fig. 4a), suggesting the formation of a low-dimensional mesophase between the solid-state and the isotropic liquid. The liquid crystalline behaviour of **FG1** was evidenced by POM observations revealing non-conventional optical texture (see Fig. 3), consisting of birefringent and fluid ribbon-like domains, coalescing into uniform micrometric monodomains on slow cooling from the isotropic liquid.

X-ray patterns of **FG1** recorded at 150 °C (Fig. 4b and S5†, ESI) in its mesophase exhibit a series of sharp and intense reflections in the small-angle range along with broad and diffuse wide-angle signals. These scatterings, referred to as I, II, and III (Fig. 4b), correspond to some weak short-range molecular fluctuations and evidence the liquid-like nature of the mesophase. The most intense halo II, located at *ca.* 4.7 Å, represents the typical correlation distance between aliphatic chains in liquid-like conformation, and is in direct line with the fluid nature of the mesophase.

The quite sharp halo I, measured at a distance of 3.7 Å is associated to close *face-to-face* (so-called π–π) stacking of the aromatic cores. Finally, the very weak halo III located at *ca.* 7.4 Å and corresponding to the doubling of the periodicity of I is tentatively interpreted as the manifestation of a pairing process resulting from loose antiparallel (alternated) π-stacking of adjacent molecules. Such interactions are possible between the fluorenone–thiophene central units due to the planar geometry of the aromatic central units as clearly observed in the view of the molecular single crystal structure of the dibrominated compound **8** (see Fig. S4† in the ESI). In the small-angle region, eight sharp Bragg reflections can be clearly observed and measured (Fig. 4, see Fig. S5† and Table S5† in the ESI). Such an X-ray pattern reflecting an apparent low symmetry is rather unusual for liquid crystalline materials. Obviously, straightforward 1D-smectic or 2D-columnar supramolecular organisations are to be excluded due to (i) the presence of numerous reflections, incompatible with the above-mentioned low-dimensional structures and (ii) the great variability of the small-angle reflections' intensity with diffraction angle, with four intense reflections (**1**, **2**, **3**, and **4**, ESI†).

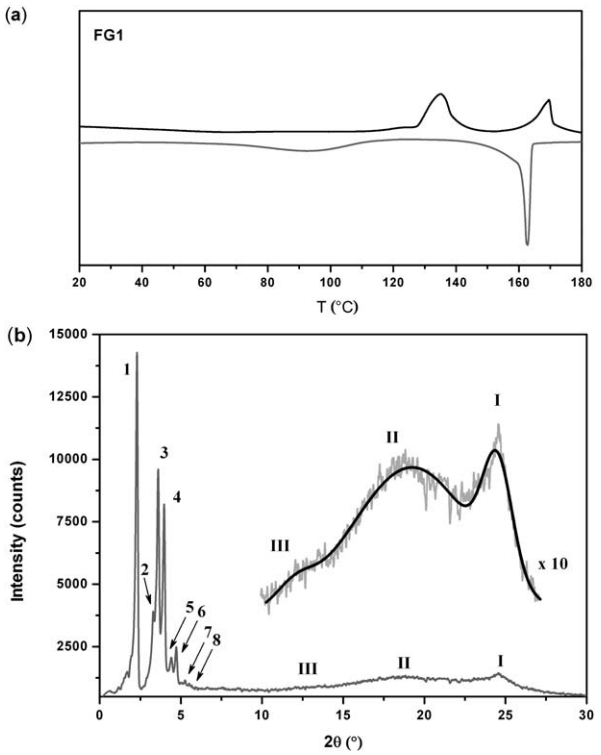

Fig. 4 a) DSC thermogram obtained during the first heating and cooling cycles at a scan rate of 5 °C min^{-1} for **FG1**, and (b) X-ray diffractograms of **FG1** in its Sm_{obl} phase at 150 °C.

In contrast, this matches well with the signatures of more complex low-symmetry three-dimensional structures. Attempted indexations into the highly symmetrical 3D orthorhombic, tetragonal, hexagonal, and cubic crystal systems obviously failed (and the corresponding space groups are therefore excluded).

Indexation in a monoclinic system also failed. The only suitable solutions for the indexation were obtained by trying serendipitously various combinations in the frame of the triclinic crystalline system ($P1$ and $P\bar{1}$ space groups). With the hypothesis that reflections **1** and **6** correspond to the lamellar stacking due to the aliphatic–aromatic alternation, the screening of all possible lattices converge with reflections **2**, **3** and **4** being the fundamental *hk*0 reflections of the oblique 2D lattice, and reflections **5**, **7** and **8** to the *hkl* satellites of the reflections with $l \neq 0$ (*i.e.* in other words reflections **5**, **7**, and **8** are compositions of 00*l* and *hk*0 reflections). All solutions give similar parameters for the triclinic lattice, and only the most representative is given here: $a = 53.6$ Å; $b = 26.3$ Å; $c = 38.7$ Å, $\alpha = 102.5°$; $\beta = 98.5°$; $\gamma = 95.5°$ and $V = 52.3\ 10^3$ Å ^{3}. The lattice, containing two elements, is filled by approximately 18 to 20 molecules assembled into bundles (with a density of 1, **FG1** has an estimated volume of *ca.* 2780 Å ^{3}). With 20 molecules in the lattice, each end-chain paves 35 Å ^{2} of the surface lattice area S ($S = ab\sin\gamma$) and the average tilt angle of the rigid part can be estimated close to 55–60° with respect to the layer normal. The mesophase with triclinic symmetry[27] may be described as an ordered 3D smectic phase with the concomitant development of both in-plane oblique symmetry and interplanar registry. The mesophase may thus be referred to as Sm_{obl}, and its structure may be compared to a crystal smectic H or K phase, but where the elementary unit

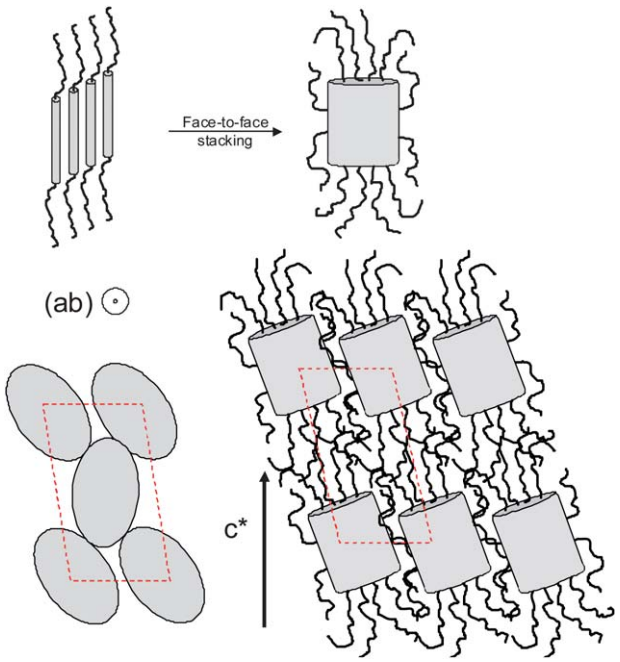

Fig. 5 Proposed model of the 3D smectic phase (Sm_{obl}) for **FG1** with *sanidic*-type bundle as mesogen units.

does not consist of a single mesogen but of a sanidic-type bundle made of a discrete number of mesogens. At the molecular level, the mesophase would result in bundles, disposed on the nodes of a triclinic network, made of few molecules (*ca.* 9–10) packed *face-to-face* in an alternated manner (*i.e.* with the antiparallel arrangement of the transverse dipole moment), with their main molecular axis oriented in the same direction, but with a angle of 55–60° with respect to the *c**-axis [001] (Fig. 5).

The segregation of the aliphatic chains induces the periodic layering of the structure. In the *ab*-plane (plane perpendicular to the layer normal *c**), the bundles are arranged according to an oblique lattice. The tilt and the bundle anisotropy are sources of disordering within the plane, and maybe the cause of the undetected higher order reflections *hk*0 of the oblique lattice.

The interlayer sliding, usually occurring in smectic phases, is frozen into an optimal lateral shift, generating the apparition of the *hkl* reflections of the triclinic lattice. The consequence of undetected *hk*0 high orders is the impossibility to describe precisely the inside of the oblique lattice, but the only information is derived from the relative low intensity of the fundamental reflection **2** with respect to **3** and **4** and implies that the weakest contrast is along the *a*-vector.

2.5. Photovoltaic properties

After their complete physico-chemical characterization, we pursued our preliminary study to test the applicability of these molecules for photovoltaic conversion.

To evaluate the photovoltaic performances of the newly synthesized fluorenone-based D–A–D molecules, we fabricated testing devices using the BHJ organic solar cells configuration with the following device architecture: glass–ITO/PEDOT:PSS/**FGX**:PCBM/LiF/Al where molecules **FGX** (X = 0, 1, 2) were

used as the electron donor and [60]PCBM or [70]PCBM as the electron acceptor components. More detail description of the device fabrication and characterization can be found in the experimental section. In order to improve the accuracy and reproducibility of the reported power conversion efficiencies for solar cells, it is crucial to avoid small cell areas (<0.2 cm^2), since it is known that efficiencies obtained on smaller areas are size-dependent and can be strongly overestimated.[28] The effective device area used in this study was 0.28 cm^2 ($\pm$0.02 cm^2).

FGX molecules were first blended with [60]PCBM in a 1 : 1 or 1 : 2 weight ratio and then the active layers were fabricated by casting from chlorobenzene solutions. Unfortunately we found that most of the organic solar cells fabricated from the 1 : 1 ratio mixtures were either in short circuit or their performances were not measurable. The performance parameters of the cells fabricated using the **FGX**:[60]PCBM ratio of 1 : 2 ratio by weight were better with a power conversion efficiency (PCE) of the order of *ca.* 0.15–0.25 % (see Table 2). Surprisingly, the cell performance could not be improved by post-annealing treatments of the complete device. To the contrary, the thermal treatment resulted in a dramatic decrease in the overall performance of the photovoltaic cells. The poor FF and the low J_{SC} measured on operating organic cells may indicate the formation of undesirable aggregates [60]PCBM (caused by its limited solubility) during the spin-coating process. This apparently leads to a blend morphology where significant phase separation favours recombination processes.

In the next part of this study, we have therefore focused our investigations on **FG1** prompted by its interesting physico-chemical and mesomorphic properties. [60]PCBM was replaced by [70]PCBM, and was reported to show higher performances.[29] In addition to a better solubility in chlorobenzene solution (up to 40 mg mL^{-1}), [70]PCBM exhibits a strong absorption band in the visible part of the spectrum that might contribute to the generation of charges and, by consequence, to an increase of the current densities delivered by the solar cells. When highly concentrated chlorobenzene solutions are used for the preparation of active layers (20 mg mL^{-1} of **FG1**), the thicknesses of films is comprised between 350 and 400 nm and the efficiency of the **FG1**:[70]PCBM device is strongly dependent on thermal annealing treatments. Table 2 summarizes some of the observed effects. An annealing temperature of 90 °C was found to be optimum despite the fact that it is much lower than the temperature at which the *crystal-to-mesophase* transition occurs

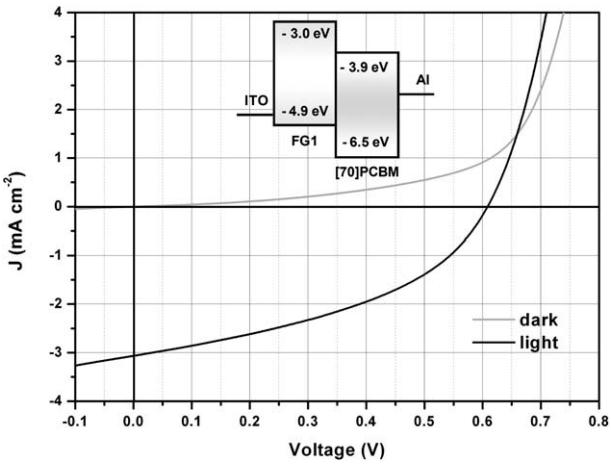

Fig. 6 Current density voltage (J–V) characteristics and energy diagram of a FG1:[70]PCBM blend. The grey line was measured in the dark, the dark line under illumination (AM 1.5, 100 mW cm^{-2}).

(Cr. 126 °C, Sm_{Obl}). Higher annealing treatments (at 120 °C or at 150 °C) resulted in less efficient solar cells. The overall effect of annealing at 90 °C was that all parameters relevant to the energy-conversion efficiency were improved. However, it should be underlined that this effect was only obtained after annealing of the complete devices. The thermal treatment resulted in an improvement of charge transport (the measured J_{sc} values were 5 to 15 times higher), and in an increase of the fill factor (Fig. 6).

The estimated potential loss of the devices were of the order of 0.2–0.4 V, in good agreement with the majority of the literature reports, where experimental V_{OC} values were found smaller than the theoretical upper value, *i.e.*, $LUMO_{([70]PCBM)}$-$HOMO_{(FG1)}$, with potential losses of *ca.* 0.3–0.4 V.

When chlorobenzene solutions with a lower concentration (12 mg mL^{-1} of **FG1**) were used for the preparation of the active layers, the thickness of the blended films was consequently reduced, typically around 90–120 nm, and increased efficiencies were observed. The current densities delivered by the photovoltaic cells raised up to 3.47 mA.cm^{-2} and the FF was slightly improved leading to a PCE value of *ca.* 0.8%. In this case, annealing treatments of the photovoltaic devices were detrimental to their performances leading to reduced electrical parameters, even after annealing at 90 °C.

Table 2 Photovoltaic properties of fluorenone-based D–A–D molecule/PCBM-based devices

Active layer (weight ratio)	Treatment/°C	V_{oc}/V	J_{sc}/mA cm^{-2}	FF	η (%)
FG0:[60]PCBM (1 : 2)[a]	As cast	0.39	0.96	35	0.13
FG1:[60]PCBM (1 : 2)[a]	As cast	0.55	1.21	36	0.24
FG2:[60]PCBM (1 : 2)[a]	As cast	0.59	0.75	32	0.14
FG1:[70]PCBM (1 : 1.5)[a]	As cast	0.53	0.42	20	0.05
FG1:[70]PCBM (1 : 1.5)[a]	5 min at 70 °C	0.61	1.90	36	0.41
FG1:[70]PCBM (1 : 1.5)[a]	5 min at 90 °C	0.56	2.15	39	0.47
FG1:[70]PCBM (1 : 1.5)[a]	5 min at 120 °C	0.50	1.22	36	0.22
FG1:[70]PCBM (1 : 2)[b]	As cast	0.58	3.47	39	0.78
FG1:[70]PCBM (1 : 2.5)[b]	As cast	0.61	3.06	42	0.78

[a] Spin-coated from chlorobenzene solution with **FG1** concentration of 20 mg mL^{-1}. [b] Spin-coated from chlorobenzene solution with **FG1** concentration of 12 mg mL^{-1}. (J_{SC}: short circuit current density, V_{OC}: open circuit voltage, FF: fill factor, η: energy conversion efficiency).

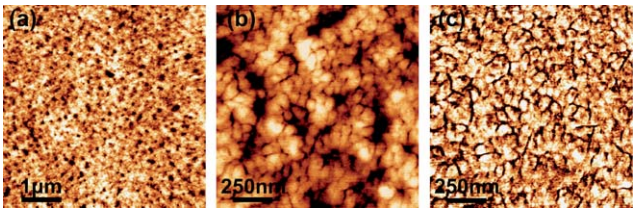

Fig. 7 AM-AFM images (ambient conditions, 512 × 512 pixels) of FG1-[70]PCBM film with a weight ratio of 1 : 2.5, as cast (a) topography, 5 μm × 5 μm. (b) topography and (c) phase, 1.25 μm × 1.25 μm.

All **FG1**:[70]PCBM thin films, *i.e.* those cast from less concentrated solutions, were very smooth and showed a nano-scale phase separation, independent of the D–A ratio in the blend (see Fig. 7).

Since the morphology of the active layer is one of the crucial parameter determining the cell performance, we have done a detailed investigation using Atomic Force Microscopy (AFM).

To the contrary the AFM images of the thicker samples revealed distinct domains in both topographical and phase images, with rectangle-shaped features. From these images, it can be inferred that the aligned fibers, which can be distinguished in the rectangle-shape features, are donor-rich domains and the light spots in the phase image structures are acceptor-rich domains (see Fig. 8a–c).

The observation of this ordered network showing a distinct phase separation may provide an explanation of the lower PCEs observed for these photovoltaics devices.

Such phase separation phenomena is obviously unfavorable for the dissociation of excitons. The images of thin films annealed at 120 °C or higher temperatures clearly demonstrate that a demixing process occurs. In this case bright spots corresponding to [70]PCBM crystallites can be clearly distinguished. This observation is fully consistent with the degradation of the electrical performance observed for the photovoltaic devices annealed at temperatures above 90 °C.

Finally, we have performed Incident Photon to Current Efficiency (IPCE) experiments. The results of the IPCE experiments

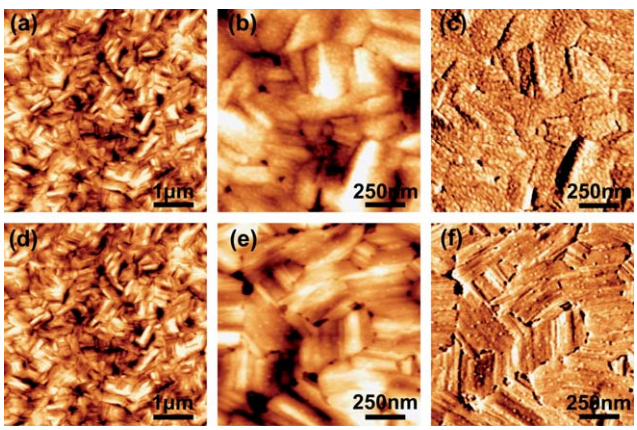

Fig. 8 AM-AFM images (ambient conditions, 512 × 512 pixels) of FG1:[70]PCBM (1 : 1.5), with different post-deposition annealing temperatures. (a, b, c) 5 mn at 90 °C. (a) Topography, 5 μm × 5μm. (b, c) topography and phase, 1.25 μm × 1.25 μm. (d, e, f) 5 mn at 120 °C. (d) Topography, 5 μm × 5 μm. (e, f) Topography and phase, 1.25 μm × 1.25 μm.

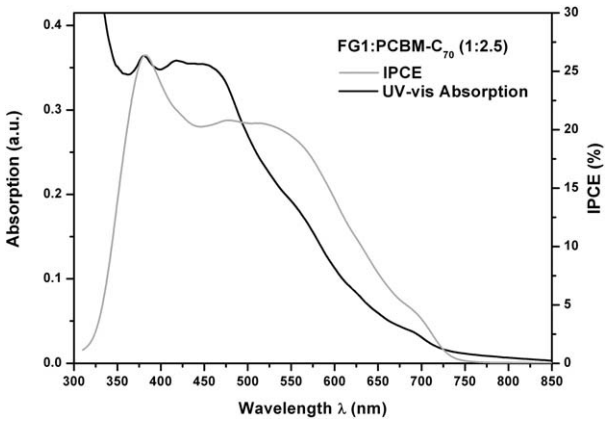

Fig. 9 Absorption spectrum of the FG1:[70]PCBM active layer (black line) and IPCE curve of the corresponding photovoltaic cell (grey line).

unequivocally confirmed the photoelectrical activity of both components of the BHJ.

The solid-state absorption spectrum of a typical **FG1**:[70]PCBM layer is shown in Fig. 9. It matches the IPCE curve which shows increased values in the spectral region (*i.e.* over 15%) where both components of the blend show high absorbance between 350 nm and 600 nm.

Interestingly, the devices can generate photocurrents of up to 750 nm. This finding unequivocally confirms active participation of the ICT absorption, resulting from the presence of the donor and acceptor segments in **FG1**, in the generation of the photocurrent.

3. Conclusions

In conclusion, molecular bulk-heterojunction solar cells have been fabricated using a novel family of D–A–D π-conjugated molecules consisting of a fluorenone core and oligothiophene dendrons of increasing generations. These molecular semiconductors show a perfectly well-defined chemical structure and can be solution processed. Among the newly synthesized molecules the organic semiconductor **FG1** revealed a liquid crystalline behaviour corresponding to a smectic ordering with a triclinic symmetry (Sm_{obl}) upon heating. This compound was blended with [70]PCBM to fabricate solar cells. Test devices of an active area of 0.28 cm^2 showed PCE values up to *ca.* 0.8%.

4. Experimental

Details related to the solar cell device fabrication, analytical procedures, and used chemicals can be found in the ESI†.

Syntheses

2,7-Bis(4,5″-dioctyl-[5,2′;5′,2″]-terthiophen-2-yl)-fluoren-9-one (FG0). Palladium tetrakistriphenyl phosphine ($Pd(PPh_3)_4$, 22 mg, 0.019 mmol, 4% molar) was added to a DMF solution (30 mL) containing **2** (1.15 mmol, 2.4 eq.) and **9** (470 mg, 0.477 mmol, 1 eq.). The reaction mixture was stirred for 14 hours at 100 °C and then allowed to cool to room temperature. The crude mixture was extracted with chloroform, washed with 2 N HCl aqueous solution, and filtered through celite. The organic layer was dried over Na_2SO_4 and concentrated under

vacuum. The crude product was purified by column chromatography on silica gel using chloroform as eluent. A second purification by column chromatography using mixtures of solvents of increasing polarity (hexane/chloroform 100/10 to 70/30 v/v) afforded the desired product **FG0** as a red-purple solid (89%, 480 mg). Employing the same procedure, starting from **8**, the product was obtained with a yield of 50%. ^{1}H NMR (200 MHz, $CDCl_3$) δ (ppm): 7.82 (d, $^5J = 1.5$ Hz, 2H), 7.61 (dd, $^3J = 7.7$ Hz and $^5J = 1.7$ Hz, 2H), 7.41 (d, $^3J = 7.8$ Hz, 2H), 7.18 (s, 2H), 7.03 (d, $^3J = 3.8$ Hz, 2H), 7.00 (d, $^3J = 3.6$ Hz, 2H), 6.99 (d, $^3J = 3.5$ Hz, 2H), 2.79 (t, $^3J = 7.6$ Hz, 4H), 2.75 (t, $^3J = 7.7$ Hz, 4H), 1.75–1.61 (m, $^3J = 7.6$ Hz, 8H), 1.43–1.22 (m, 40H), 0.89 (t, $^3J = 6.6$ Hz, 12H). ^{13}C NMR ($CDCl_3$, 50 MHz): δ (ppm): 193.28 (C=O), 145.62 (2C), 142.54 (2C), 140.48 (2C), 140.02 (2C), 137.76 (2C), 134.97 (2C), 134.79 (2C), 134.37 (2C), 134.14 (2C), 131.05 (2C), 130.89 (2C), 126.66 (2C), 126.24 (2C), 124.79 (2C),123.33 (2C), 123.17 (2C), 120.79 (2C), 120.68 (2C), 31.91 (2C), 31.86 (2C), 31.60 (2C), 30.46 (2C), 30.21 (2C), 29.63 (4C), 29.45 (2C), 29.34 (2C), 29.30 (2C), 29.24 (2C), 29.12 (2C), 22.70 (2C), 22.67 (2C), 14.14 (2C), 14.11 (2C). HRMS [M$^{+\bullet}$] ion *m*/*z* 1120.4: $C_{69}H_{84}OS_6$, *m*/*z* calculated 1120.4841, *m*/*z* found: 1120.4826.

2,7-Bis(5-[3,5‴-dioctyl-4″-(5-octylthien-2-yl)-[2,2′;5′,2″;5″,2‴]-quaterthiophene])-fluoren-9-one (FG1). Palladium tetrakistriphenylphosphine ($Pd(PPh_3)_4$, 33 mg, 0.028 mmol, 4% molar) was added to a DMF solution containing **4** (1.68 mmol, 2.4 eq.) and **9** (700 mg, 0.71 mmol). The reaction mixture was stirred for 14 hours at 100 °C and then allowed to cool to room temperature. The crude mixture was extracted with chloroform, washed with HCl 2N aqueous solution, and filtered through celite. After usual work-up, the crude product was purified by column chromatography on silica gel with mixture of solvents hexane–chloroform 90/10 to 65/35 v/v). The product after evaporation of the solvent was dissolved in pure chloroform and precipitated from acetone. After filtration and drying under vacuum, **FG1** was obtained as a deep red-brown wax (75%, 890 mg). ^{1}H NMR (200 MHz, $CDCl_3$) δ (ppm): 7.75 (d, $^5J = 1.2$ Hz, 2H), 7.53 (dd, $^3J = 7.6$ Hz and $^5J = 1.2$ Hz, 2H), 7.34 (d, $^3J = 7.7$ Hz, 2H), 7.13 (s, 4H), 7.05 (d, $^3J = 3.8$ Hz, 2H), 6.98 (d, $^3J = 3.8$ Hz, 2H), 6.93 (d, $^3J = 3.5$ Hz, 2H), 6.89 (d, $^3J = 3.5$ Hz, 2H), 6.67 (d, $^3J = 3.5$ Hz, 2H), 6.65 (d, $^3J = 3.5$ Hz, 2H), 2.75 (m, $^3J = 7.1$ Hz, 12H), 1.69–1.56 (m, $^3J = 7.1$ Hz, 12H), 1.45–1.20 (m, 60H), 0.89 (t, $^3J = 6.6$ Hz, 18H). ^{13}C NMR ($CDCl_3$, 50 MHz): δ (ppm): 193.33 (C=O), 147.62 (2C), 146.47 (2C), 142.64 (2C), 140.72 (2C), 140.28 (2C), 136.42 (2C), 135.29 (2C), 135.05 (2C), 134.77 (2C), 134.75 (2C), 134.50 (2C), 132.36 (2C), 132.22 (2C), 131.10 (2C), 130.83 (4C), 127.44 (4C), 126.76 (2C), 126.56 (2C), 126.30 (2C), 126.16 (2C), 124.29 (2C), 124.16 (4C), 120.79 (2C), 32.05 (2C), 30.00 (4C), 31.77 (2C), 31.67 (2C), 30.53 (2C), 30.29 (2C), 30.27 (2C), 29.82 (4C), 29.62 (2C), 29.48 (2C), 29.46 (4C), 29.39 (4C), 29.27 (4C), 22.84 (2C), 22.80 (4C), 14.27 (2CH_3), 14.23 (4CH_3). HMRS [M$^{+\bullet}$] ion *m*/*z* 1672.7: $C_{101}H_{124}OS_{10}$, *m*/*z* calculated 1672.68539, *m*/*z* found: 1672.6852.

2,7-Bis(5-[3,5‴′-dioctyl-4″-(5′,5″-dioctyl-2,2′:3,2″-terthio-phen-5-yl)-4‴-(5-octylthien-2-yl)-[2,2′;5′,2″;5″,2‴;5‴, 2‴′]pentathiophene])-fluoren-9-one (FG2). Palladium tetrakistriphenylphosphine ($Pd(PPh_3)_4$, 15 mg, 0.013 mmol, 4% molar) was added to a DMF solution containing **6** (0.77 mmol, 2.4 eq.) and **9** (320 mg, 1 eq., 0.32 mmol). The reaction mixture was stirred for 14 hours at 100 °C and then allowed to cool to room temperature. The crude mixture was extracted with diethylether, washed with HCl 2N aqueous solution, and filtered through celite. The organic layer was dried over Na_2SO_4 and concentrated under vacuum. The crude product was purified by column chromatography on silica gel with mixtures of solvents of increasing polarity: hexane/chloroform 100/0 to 60/40 v/v). **FG2** was obtained as a brown wax (48%, 435 mg). ^{1}H NMR (200 MHz, $CDCl_3$) δ (ppm): 7.83 (d, $^5J = 1.2$ Hz, 2H), 7.62 (dd, $^3J = 7.8$ Hz and $^5J = 1.2$ Hz, 2H), 7.43 (d, $^3J = 7.8$ Hz, 2H), 7.22 (s, 2H), 7.21 (s, 2H), 7.19 (s, 2H), 7.18 (s, 2H), 7.11 (d, $^3J = 3.8$ Hz, 2H), 7.03 (d, $^3J = 3.8$ Hz, 2H), 6.95 (d, $^3J = 3.7$ Hz, 2H), 6.93 (d, $^3J = 3.7$ Hz, 2H), 6.87 (d, $^3J = 3.5$ Hz, 2H), 6.86 (d, $^3J = 3.5$ Hz, 2H), 6.65 (d, $^3J = 3.4$ Hz, 4H), 6.66 (d, $^3J = 3.4$ Hz, 4H), 2.76 (t, $^3J = 7.3$ Hz, 20H), 1.70–1.50 (m, $^3J = 7.1$ Hz, 20H), 1.50–1.15 (m, 100H), 0.88 (t, $^3J = 6.1$Hz, 30H). ^{13}C NMR ($CDCl_3$, 50 MHz): δ (ppm): 193.19 (C=O), 147.61 (2C), 146.45 (2C), 146.77 (2C), 146.13 (2C), 142.51 (2C), 140.59 (2C), 140.19 (2C), 140.00 (2C), 139.70 (2C), 135.71 (2C), 135.64 (2C), 134.99 (2C), 134.90 (2C), 134.71 (2C), 134.54 (2C), 134.37 (2C), 132.82 (2C), 132.34 (2C), 132.15 (2C), 131.98 (2C), 131.92 (2C), 131.83 (2C), 131.54 (2C), 131.06 (2C), 130.63 (2C), 130.07 (2C), 129.75 (2C), 127.51 (2C), 127.47 (2C), 126.51 (2C), 126.39 (2C), 126.23 (2C), 126.09 (2C), 125.79 (2C), 125.64 (2C), 124.34 (4C), 124.13 (2C), 123.99 (4C), 120.67 (2C), 120.58 (2C), 31.88 (10C), 31.64 (4C), 31.54 (4C), 30.56 (1C), 30.35 (1C), 30.16 (6C), 29.73 (2C), 29.53 (2C), 29.34 (10C), 29.27 (10C), 29.15 (10C), 22.67 (10C), 14.11 (10C). HMRS [M$^{+\bullet}$] ion *m*/*z* 2777.1: $C_{165}H_{204}OS_{18}$, *m*/*z* calculated 2777.0885, *m*/*z* found: 2777.0884.

Acknowledgements

The authors thank ANR and CNRS for funding through the Nanorgasol (ANR) and Programme Interdisciplinaire Energie Celasol (CNRS) research programs. RD and FL thank CEA for financial support. Yann Kervella, Dr Solenn Berson, Séverine Bailly and Zaireen Yahya are also acknowledged for technical assistance.

References

1 (*a*) H. Hoppe and N. S. Sariciftci, *J. Mater. Res.*, 2004, **19**, 1924; (*b*) Y.-J. Cheng, S.-H. Yang and C.-S. Hsu, *Chem. Rev.*, 2009, **109**, 5868; (*c*) L.-M. Chen, Z. Hong, G. Li and Y. Yang, *Adv. Mater.*, 2009, **21**, 1434.
2 (*a*) U. Mitschke and P. Bäuerle, *J. Mater. Chem.*, 2000, **10**, 1471; (*b*) A. C. Grimsdale, K. L. Chan, R. E. Martin, P. G. Jokisz and A. B. Holmes, *Chem. Rev.*, 2009, **109**, 897.
3 (*a*) C. D. Dimitrakopoulos and P. R. L. Malenfant, *Adv. Mater.*, 2002, **14**, 99; (*b*) H. E. Katz, Z. N. Bao and S. L. Gilat, *Acc. Chem. Res.*, 2001, **34**, 359; (*c*) A. Pron, P. Gawrys, M. Zagorska, D. Djurado and R. Demadrille, *Chem. Soc. Rev.*, 2010, **39**, 2577.
4 (*a*) G. Dennler, M. C. Scharber and C. J. Brabec, *Adv. Mater.*, 2009, **21**, 1323; (*b*) B. C. Thompson and J. M. J. Fréchet, *Angew. Chem., Int. Ed.*, 2008, **47**, 58.
5 (*a*) R. Steima, P. Schilinsky, S. A. Choulis and C. J. Brabec, *Sol. Energy Mater. Sol. Cells*, 2009, **93**, 1963; (*b*) V. Shrotriya, *Nat. Photon.*, 2009, **3**, 447.
6 (*a*) M. T. Lloyd, J. E. Anthony and G. G. Malliaras, *Mater. Today*, 2007, **10**, 34; (*b*) J. Roncali, *Acc. Chem. Res.*, 2009, **42**, 1719.
7 (*a*) A. B. Tamayo, X.-D. Dang, B. Walker, J. Seo, T. Kent and T.-Q. Nguyen, *Appl. Phys. Lett.*, 2009, **94**, 103301; (*b*) T. Rousseau, A. Cravino, T. Bura, G. Ulrich, R. Ziessel and J. Roncali, *J. Mater.*

Chem., 2009, **19**, 2298; (*c*) B. Walker, A. B. Tamayo, X.-D. Dang, P. Zalar, J. H. Seo, A. Garcia, M. Tantiwiwat and T.-Q. Nguyen, *Adv. Funct. Mater.*, 2009, **19**, 3063; (*d*) M. Velusamy, J.-H. Huang, Y.-C. Hsu, H.-H. Chou, K.-C. Ho, P.-L. Wu, W.-H. Chang, J. T. Lin and C.-W. Chu, *Org. Lett.*, 2009, **11**, 4898; (*e*) T. Rousseau, A. Cravino, T. Bura, G. Ulrich, R. Ziessel and J. Roncali, *Chem. Commun.*, 2009, 1673.

8 A. Mishra, C.-Q. Ma and P. Bäuerle, *Chem. Rev.*, 2009, **109**, 1141.

9 (*a*) W. W. H. Wong, C.-Q. Ma, W. Pisula, C. Yan, X. Feng, D. J. Jones, K. Müllen, R. A. J. Janssen, P. Bäuerle and A. B. Holmes, *Chem. Mater.*, 2010, **22**, 457; (*b*) J.-L. Wang, C. M. Zhong, Z. M. Tang, H. B. Wu, Y. G. Ma, Y. Cao and J. Pei, *Chem. Asian J.*, 2010, **5**, 105.

10 N. Kopidakis, W. J. Mitchell, J. van de Lagemaat, D. S. Ginley, G. Rumbles and S. E. Shaheen, *Appl. Phys. Lett.*, 2006, **89**, 103524.

11 (*a*) M. K. R. Fischer, T. E. Kaiser, F. Würthner and P. Bauerle, *J. Mater. Chem.*, 2009, **19**, 1129; (*b*) B. L. Rupert, W. J. Mitchell, A. J. Ferguson, M. E. Köse, W. L. Rance, G. Rumbles, D. S. Ginley, S. E. Shaheen and N. Kopidakis, *J. Mater. Chem.*, 2009, **19**, 5311; (*c*) G. Ramankrishna, A. Bhakar, P. Bauerle and T. Goodson,III, *J. Phys. Chem. A*, 2008, **112**, 2018.

12 (*a*) S. Roquet, A. Cravino, P. Leriche, O. Aleveque, P. Frere and J. Roncali, *J. Am. Chem. Soc.*, 2006, **128**, 3459; (*b*) Y. Li, L. Xue, H. Li, Z. Li, B. Xu, S. Wen and W. Tian, *Macromolecules*, 2009, **42**, 4491.

13 (*a*) C. Xia, X. Fan, J. Locklin and R. Advincula, *Org. Lett.*, 2002, **12**, 2067; (*b*) W. J. Mitchell, N. Kopidakis, G. Rumbles, D. S. Ginley and S. E. Shaheen, *J. Mater. Chem.*, 2005, **15**, 4518.

14 R. Demadrille, N. Delbosc, Y. Kervella, M. Firon, R. De Bettignies, M. Billon, P. Rannou and A. Pron, *J. Mater. Chem.*, 2007, **17**, 4661.

15 L. J. Andrews, A. Deroulede and H. Linschitz, *J. Phys. Chem.*, 1978, **82**, 2304.

16 (*a*) F. Jaramillo-Isaza and M. L. Turner, *J. Mater. Chem.*, 2006, **16**, 83; (*b*) M. Y. Odoi, N. I. Hammer, H. P. Rathnayake, P. M. Lahti and M. D. Barnes, *ChemPhysChem.*, 2007, **8**, 1481; (*c*) A. Demeter, G. Timfiri, A. Kotschy and T. Berces, *Tetrahedron Lett.*, 1997, **38**(29), 5219.

17 R. Demadrille, P. Rannou, J. Bleuse, J.-L. Oddou, A. Pron and M. Zagorska, *Macromolecules*, 2003, **36**, 7045.

18 T. Benincori, M. Capaccio, F. De Angelis, L. Falciola, M. Muccini, P. Mussini, A. Ponti, S. Toffanin, P. Traldi and F. Sannicolo, *Chem. Eur. J.*, 2008, **14**, 459.

19 Y. Zhang, C. Zhao, J. Yang, M. Kapiamba, O. Haze, L. J. Rothberg and M.-K. Ng, *J. Org. Chem.*, 2006, **71**, 9475.

20 (*a*) C.-Q. Ma, M. Fonrodona, M. C. Schikora, M. M. Wienk, R. A. J. Janssen and P. Bäuerle, *Adv. Funct. Mater.*, 2008, **18**, 3323; (*b*) C. Xia, X. Fan, J. Locklin, R. C. Advincula, A. Gies and W. Nonidez, *J. Am. Chem. Soc.*, 2004, **126**, 8735.

21 (*a*) P. J. Brown, D. S. Thomas, A. Köhler, J. S. Wilson, J.-S. Kim, C. M. Ramsdale, H. Sirringhaus and R. H. Friend, *Phys. Rev. B*, 2003, **67**, 064203; (*b*) T. Yamamoto, D. Komarudin, M. Arai, B. L. Lee, H. Suganuma, N. Asakawa, Y. Inoue, K. Kubota, S. Sasaki, T. Fukuda and H. Matsuda, *J. Am. Chem. Soc.*, 1998, **120**, 2047; (*c*) B. Grevin, R. Demadrille, M. Linares, R. Lazzaroni and P. Leclere, *Adv. Mater.*, 2009, **21**, 4124.

22 F. Uckert, S. Setavesh and K. Müllen, *Macromolecules*, 1999, **32**, 4519.

23 (*a*) T. Johansson, W. Mammo, M. Svensson, M. R. Andersson and O. Inganäs, *J. Mater. Chem.*, 2003, **13**, 1316; (*b*) I. Polec, A. Henckens, L. Goris, M. Nicolas, M. A. Loi, P. J. Adriaensens, L. Lutsen, J. V. Manca, D. Vanderzande and N. S. Sariciftci, *J. Polym. Sci., Part A: Polym. Chem.*, 2003, **41**, 1034.

24 (*a*) M.-T. Escota, P. Pouillen and P. Martinet, *Electrochim. Acta*, 1983, **28**, 1697; (*b*) A. Cihaner, S. Tirkes and A. M. Onal, *J. Electroanal. Chem*, 2004, **568**, 151.

25 (*a*) C. J. Brabec, A. Cravino, D. Meissner, N. S. Sariciftci, T. Fromherz, M. T. Rispens, L. Sanchez and J. C. Hummelen, *Adv. Funct. Mater.*, 2001, **11**, 374; (*b*) F. B. Kooistra, V. D. Mihailetchi, L. M. Popescu, D. Kronholm, P. W. M. Blom and J. C. Hummelen, *Chem. Mater.*, 2006, **18**, 3068.

26 J. J. M. Halls, J. Cornil, D. A. dos Santos, R. Silbey, D.-H. Hwang, A. B. Holmes, J. L. Brédas and R. H. Friend, *Phys. Rev. B*, 1999, **60**, 5721.

27 K. Oikawa, H. Monobe, K.-I. Nakayama, T. Kimoto, K. Tsuchiya, B. Heinrich, D. Guillon, Y. Shimizu and M. Yokoyama, *Adv. Mater.*, 2007, **19**, 1864.

28 (*a*) A. K. Pandey, J. M. Nunzi, B. Ratier and A. Moliton, *Phys. Lett. A*, 2008, **372**, 1333; (*b*) D. Gupta, M. Bag and K. S. Narayan, *Appl. Phys. Lett.*, 2008, **93**, 163301.

29 P. A. Troshin, H. Hoppe, J. Renz, M. Egginger, J. Yu. Mayorova, A. E. Goryachev, A. S. Peregudov, R. N. Lyubovskaya, G. Gobsch, N. S. Sariciftci and V. F. Razumov, *Adv. Funct. Mater.*, 2009, **19**, 779.